BNL-108561-2015-JA

WILEY-VCH

DOI: 10.1002/((please add manuscript number))
Article type: Communication

Guided Evolution of Bulk Metallic Glass Nanostructures: A Platform for Designing Three-Dimensional Electrocatalytic Surfaces

*Gustavo Doubek†, Ryan C. Sekol†, Jinyang Li†, Won-Hee Ryu, Forrest S. Gittleson, Siamak Nejati, Eric Moy, Candy Reid, Marcelo Carmo, Marcelo Linardi, Punnathat Bordeenithikasem, Emily Kinser, Yanhui Liu, Xiao Tong, Chinedum Osuji, Jan Schroers, Sundeep Mukherjee, and André D. Taylor**

† *These authors contributed equally to this work.*

Addresses and Affiliations when the work was carried out:

Dr. G. Doubek, Dr. R. C. Sekol, J. Li, Dr. W.-H. Ryu, Dr. F. S. Gittleson, Dr. S. Nejati, E. Moy, C. Reid, Dr. M. Carmo, Prof. C. Osuji, Prof. A. D. Taylor
Department of Chemical and Environmental Engineering
Yale University
New Haven, CT, USA 06520
E-mail: andre.taylor@yale.edu

Dr. G. Doubek, Dr. R. C. Sekol, J. Li, Dr. S. Nejati, E. Moy, C. Reid, Dr. M. Carmo, P. Bordeenithikasem, E. Kinser, Dr. Y. Liu, Dr. S. Mukherjee, Prof. C. Osuji, Prof. J. Schroers, Prof. A. D. Taylor
Center for Research on Interface Structures and Phenomena
Yale University
New Haven, CT, USA 06520

P. Bordeenithikasem, E. Kinser, Dr. Y. Liu, Prof. J. Schroers
Department of Mechanical Engineering and Materials Science
Yale University
New Haven, CT, USA 06520

Dr. G. Doubek and Prof. Marcelo Linardi
Hydrogen and Fuel Cell Center, Nuclear and Energy Research Institute
IPEN/CNEN
SP. Av. Prof. Lineu Prestes, 2242, Cidade Universitária Lineu Prestes Cidade Universitária, São Paulo
SP, Brazil 05508-000

Dr. X. Tong
Center for Functional Nanomaterials
Brookhaven National Laboratory
Upton, New York 11973, United States

Current Addresses and Affiliations:

Prof. G. Doubek
University of Campinas (UNICAMP)

School of Chemical Engineering, Campinas
SP, Brazil, 13083-852

Dr. R. C. Sekol
General Motors Research and Development
Warren, MI, USA 48090

Dr. F. S. Gittleson
Sandia National Laboratories, Livermore, CA USA 94550

Dr. M. Carmo
Forschungszentrum Julich, (IEK-3)
Julich, Germany 52428

Prof. S. Mukherjee,
Department of Materials Science and Engineering
University of North Texas
Denton, TX, USA 76203

Keywords: bulk metallic glass, nanomaterial, electrocatalyst, surface modification, pesudocapacitor

Abstract

Precise control over catalyst surface composition and structure is necessary to improve the function of electrochemical systems. To that end, bulk metallic glass (BMG) alloys with atomically dispersed elements provide a highly processable, nanoscale platform for electrocatalysis and surface modification. Here we report on nanostructures of Pt-based BMGs that are modified with various subtractive and additive processes to improve their electrochemical performance. Subtractive dealloying from multi-component BMGs yields three-dimensional nanoporous structures with increased electrochemical surface area and superior durability for hydrogen oxidation and oxygen reduction. Additive modification by underpotential deposition or galvanic displacement enriches BMG surfaces with elements that are not possible to integrate otherwise (i.e. Ru) for improved methanol oxidation. Electrodeposition of MnO_x for pseudo-capacitance capitalizes on the high surface area of BMG nanorod scaffolds for enhanced charge storage. Applying these various surface

modification techniques to nanostructured bulk metallic glasses provides a new strategy for the development of electrochemically active surfaces.

Introduction

Electrocatalysts play a central role in energy conversion and storage technologies including fuel cells[1], electrolysis cells[2] and metal–air batteries[3]. The most effective of these catalysts (i.e. Pt, Pd), however, are expensive and scarce, limiting their practical use. Much effort has been devoted to minimizing or eliminating precious metals[4], frequently through the design of alloys with metal-metal or metal-metal oxide interfaces[5]. Conveniently, multi-component catalysts can be designed to promote reactant adsorption or product desorption on their surfaces while simultaneously improving material utilization[6]. In this report, we present a unique strategy to create and tune electrochemically active surfaces using a platform of metallic glass nanostructures.

Designing multi-component catalytic surfaces to improve activity, utilization, efficiency and durability has traditionally been conducted through bulk nanoparticle synthesis[7] or surface modification[8]. While nanoparticle catalysts are preferred for their large surface areas and high activities, generating new multi-component particles with a desired morphology, composition and atomic surface structure remains more art than science[9]. Well-mixed (atomically-disperse) alloys[10] and core-shell nanoparticles[11] have shown promise for various electrochemical reactions including hydrogen evolution, oxygen reduction, and alcohol and CO oxidation, yet close control over particle surfaces during synthesis is difficult to achieve. Modifying these surfaces by post-synthesis processing is another route to enhance activity, but may yield unstable structures[12]. Here we show that it is possible to improve the catalytic function and durability of nanostructured bulk metallic glasses through compositional and morphological control.

Bulk metallic glasses (BMGs) are amorphous metallic alloys produced in volume by melting and thermal quenching. BMGs exhibit desirable properties like high strength and good formability (at reduced temperatures vs. pure metals), which make them ideal for applications like nanoimprint lithography[13], plastic-replacement components[14], and field electron emission devices[15]. The ability to nanomold BMGs[13] is particularly interesting for catalytic applications where high surface areas are necessary. We previously demonstrated Pt-BMG nanorod arrays as catalysts for oxygen reduction and Pd-BMG arrays for alcohol oxidation[16-18, 19]. Other groups have similarly demonstrated the use of Pd-based BMGs for electrocatalysis[20],[21]. While BMGs are typically composed of 3-5 elements including Pt, Pd, Au, Si, Ni, Cu, P, and Zr, many favorable BMG compositions may yet be discovered[22, 23]. We recently demonstrated a high throughput screening technique to identify some of these systems[24]. Nevertheless, the discovery of new electroactive BMG surfaces should not be limited by bulk synthesis techniques.

In this work, we demonstrate several strategies of subtractive and additive surface modification on BMG surfaces to form unique morphologies and compositions by post-processing. Subtractive modification involves dealloying of non-functional components to enrich Pt-BMG surfaces with Pt and increase surface areas through pore formation. Additive modification is accomplished with underpotential deposition, galvanic displacement and electrodeposition to introduce new species (Ru and MnO_x) to the BMG surface. We demonstrate the efficacy of these methods for the catalysis of hydrogen oxidation (HOR), oxygen reduction (ORR) and methanol oxidation (MOR), and in pseudo-capacitive electrodes. Our results show that bulk metallic glass nanostructure modification is an effective and versatile platform for the design of electrochemically active surfaces.

Results and Discussion

Subtractive Modification: Dealloying

The surface modification method known as dealloying has received much attention for its potential to change the surface area and composition of catalyst particles[25]. With this method, less noble metals (i.e. Cu, Ni, Co) are leached from a surface during electrochemical cycling, forming a porous interface enriched with noble metal sites (Figure 1a)[26],[27]. In our previous reports, we noted the effect of dealloying a $Pt_{57.5}Cu_{14.7}Ni_{5.3}P_{22.5}$ BMG (Pt-BMG(57)) on the catalytic activity for oxygen reduction and alcohol oxidation[16]. By further tailoring the dealloying process in BMGs, we can discover even more effective catalytic surfaces.

To investigate the tuning of catalytic surfaces by dealloying, we started with a Pt-Ni-Cu alloy composition similar to the Pt-BMG(57), reported previously. All alloy systems that exhibit selective leaching of a less-noble species have a "parting limit," an upper bound of the noble metal composition above which selective dealloying does not occur[28]. This limit separates the compositions in which pore formation leads to increased surface areas, and the compositions in which high surface concentrations of noble metal limit dealloying [29, 30]. To map the parting limit for the Pt-Ni-Cu system, we used a compositional spread[24] of discrete thin film patches, prepared by co-sputtering. The Pt content ranged from 25 to 82 at%, determined by energy dispersive X-ray spectroscopy (EDX). Potentiostatic cycling was carried out in 0.5 M H_2SO_4 on the entire Pt-Ni-Cu combinatorial library to determine the extent of noble metal surface enrichment for each composition (Figure 1b). Pt enrichment was found to be negligible above 70-80 at% Pt (the parting limit) and is more pronounced for lower initial Pt content. The roughly linear relationship between initial Pt content (C_{Pt}^0, at.%) and the change in Pt content (ΔC_{Pt}, at.%) is related to the initial Cu and Ni content since Cu and Ni are selectively leached during electrochemical cycling.

$C_{Pt}^0 = 100 - C_{Cu}^0 - C_{Ni}^0$ (1)

$\Delta C_{Pt} = -(\Delta C_{Cu} + \Delta C_{Ni})$ (2)

To the best of our knowledge this is the first time a combinatorial approach has been used to determine the parting limit of a metallic glass system. Based on these results, we prepared a new Pt-BMG composition of $Pt_{42.5}Cu_{27}Ni_{9.5}P_{21}$ (Pt-BMG(42)) which should exhibit greater dealloying than Pt-BMG(57). The DSC curve can be found in the Figure S1. We note that this new composition was selected to balance amorphous stability during processing at low quench rates and a desirable formability[13].

BMG nanorod arrays of Pt-BMG(57) and Pt-BMG(42) were formed with a previously described top-down thermoplastic molding procedure[16, 17, 19, 23, 31] and detached from discs by sonication (Figure S1). BMG nanorods were then dealloyed to show the evolution of their electrochemical surface area (ECSA) (Figure 1c). Voltammetric profiles (Figure 1d,e) were recorded every 100 cycles and the ECSA was calculated from the hydrogen desorption peaks located between -0.2 and 0.1 V vs. Ag/AgCl[32]. After only 200 cycles the ECSA of the Pt-BMG(57) stabilizes and the dealloying rate drops to nearly zero, corresponding to a passivation of the surface. In contrast, the ECSA of Pt-BMG(42) continuously increases over 2000 cycles. This corrosion behavior was also indicated by linear sweeping voltammetry (Figure S2). Interestingly, we reveal that after 2000 cycles, the ECSA of Pt-BMG(42) is approximately 10 times greater than that of Pt-BMG(57), despite the higher C_{Pt}^0 of the latter. We attribute this difference to the formation of a highly nanoporous surface through selective dissolution of Cu and Ni[17, 30, 33], as opposed to a dendritic surface structure shown in one of our previous studies with a Pd-BMG[17].

We studied the compositional structure and electronic state at the surface (~10 nm depth) of Pt-BMG(42) nanorod arrays over the course of the dealloying process by X-ray photoelectron spectroscopy (XPS) (Figure 2a-d). The Pt 4f spectra show a positive shift (+0.7 eV) of the deconvoluted Pt^0, Pt^{2+} and Pt^{4+} peaks from 0 to 1000 cycles, after which peak positions are maintained up to 2000 cycles (Figure 2a). We find that the Pt^{2+} peaks do not increase much in intensity with dealloying, consistent with our previous result[16], and we therefore expect no significant formation of PtO on the surface. Two small peaks near 73.5 eV and 78 eV are slightly increased after 2000 cycles, which corresponds to further oxidation to Pt^{4+}. The XPS spectra of Ni, Cu and P show that these elements are all removed from the Pt-BMG(42) surface after 1000 cycles through selective leaching (Figs. 2b-d). The positive shift of Pt^0, Pt^{2+} and Pt^{4+} peaks after 1000 cycles is therefore attributable to the decreased coordination with Ni, Cu and P, causing outer shell Pt electrons to be more strongly bound to their own nuclei. In contrast, our previous study with Pt-BMG(57) showed that Ni and Cu gradually dissolve but remain on the surface after 2000 cycles[16]. Although Pt-BMG(42) contains less Pt initially, its surface after cycling appears to exhibit more available Pt sites than the comparable Pt-BMG(57), agreeing with the higher ECSA values for Pt-BMG(42) seen in Figure 1c.

We also investigated the structural and compositional changes in Pt-BMG(42) nanorods using transmission electron microscopy (TEM) (Fig.2e-g) and EDX line scans (Figure 2h-j) at different dealloying states. We observe that dealloying of Pt-BMG(42) nanorods occurs from the surface inward and leads to fully porous nanostructures after 2000 cycles. Previous studies have indicated that when dealloying two-component nanoparticles, porous structures may collapse and lose the benefit of their high surface areas[34]. We confirm no significant collapse with our dealloyed Pt-BMG(42) nanorod arrays, suggesting good long-term durability. From EDX line scans (Figure 2h-j), we observe that Ni and Cu are progressively leached away from the BMG nanorod structure over 2000 cycles while Pt and P largely remain (Figure 2e-g).

Contrasting the presence of P after dealloying in line scan data with its absence in XPS data, we attribute this discrepancy to a bulk vs. surface concentration effect. Phosphorus may be less stabilized by inter-atomic coordination at the nanorod surface than in the interior, making it more prone to removal at the surface during electrochemical cycling. Taken together, the XPS and EDX data verify that Pt-BMG compositions further from the parting limit result in significantly higher ECSAs after subtractive modification due to Pt enrichment and pore formation.

We investigated the efficacy of freestanding Pt-BMG(42) nanorods for hydrogen oxidation at room temperature and using an accelerated durability test (ADT) at 80°C. Results were compared with those from a conventional carbon-supported Pt/C catalyst[35] (Figure 3a). Our data show that the nanostructured Pt-BMG is more stable in ECSA over 2000 cycles than a carbon-supported catalyst. In fact, due to progressive dealloying, Pt-BMG(42) can be viewed as a "self-improving" surface that reveals more active sites in response to corrosion. The effect of higher temperatures (80°C vs. 25°C) on material stability provides an even more pronounced differentiation. After ~1500 cycles at 80°C no hydrogen desorption peaks are present with Pt/C, indicating its complete deactivation. Either complete dissolution or electrical isolation of noble metal nanoparticles due to carbon corrosion[36] are likely to blame for the poor durability, but this phenomenon is not observed with freestanding Pt-BMG(42) nanorods. Given the impressive stability of Pt-BMG(42), modified BMG nanostructures may be better able to meet the U.S. Department of Energy 2017 fuel cell commercialization goals than conventional catalysts.[5]

Since Pt-containing surfaces are also commonly used to catalyze oxygen reduction, we evaluated the effectiveness of Pt-BMG(42) nanorods for this reaction and compared the activity to that of Pt/C (Figure 3b). We show that the specific activity for Pt-BMG(42)-

catalyzed ORR is nearly three times that of Pt/C (~0.3 vs. 0.1 A m_{Pt}^{-2}) and is only slightly reduced (by ~15%) after an accelerated durability test (Figure 3b). While mass activity of Pt-BMG(42) is less than Pt/C initially (~3 vs. ~5 A g_{Pt}^{-1}), after 2000 cycles there is only a minimal loss in mass activity for Pt-BMG(42) while Pt/C demonstrates a significant decrease (of ~30%). The instability of Pt/C is also illustrated by a negative shift of 73 mV in reduction onset potential after 2000 cycles (Figure S3a). For Pt-BMG(42) there is no appreciable change in onset, indicating a stable Pt surface. Koutecky-Levich plots of these materials show that the preferred ORR mechanism in both materials is a four electron reaction pathway, consistent with Pt catalysis of ORR (Figure S3b)[37].

Subtractive modification of BMGs by dealloying offers the potential to create large area, enriched surfaces that are active for a number of electrocatalytic applications. Though we have concentrated here on Pt-BMGs, similar design and tailoring can be conducted with BMGs containing a combination of noble and non-noble elements.

Additive Modification: Underpotential Deposition

Additive surface modifications can be made with several different chemical and electrochemical methods where the conditions and order of techniques have a profound influence on the final chemistry. Such modifications applied to the large compositional family of BMGs can produce a wide variety of catalytic surfaces. Techniques such as underpotential deposition, galvanic displacement and electrodeposition all allow fine control over morphology and composition. By tailoring Pt-BMG catalysts with additive modifications we reveal that it is possible to create electrocatalytic surfaces having elements outside of the metallic glass formability regime (i.e. Ru).

PtRu bimetallic nanoparticles, with superior activity and CO poisoning tolerance compared to Pt, have been identified as promising methanol oxidation catalysts for use in direct methanol fuel cells (DMFCs)[38]. The mechanistic advantage of Ru originates in ligand, geometric, or ensemble effects[39] where Ru is capable of providing oxygenate species at lower overpotentials than Pt, thus facilitating alcohol oxidation[40]. In the absence of previous reports demonstrating the synthesis of Pt- and Ru-containing metallic glasses, we investigated several methods to incorporate Ru onto Pt-BMG(42) nanorod surfaces for enhanced methanol oxidation activity and stability. Ru was added to dealloyed BMG nanorods by underpotential deposition (UPD) and to pristine BMG nanorods by (electroless) galvanic displacement (GD) with Ni and Cu (Figure 4a). Nanorods were then characterized by XPS, TEM and EDX to determine the nature of Ru integration. XPS spectra of the Ru 3d region verify that Ru/RuO_x (~281.6 eV)[41] is successfully deposited onto the Pt-BMG surface using the UPD and GD methods (Figure 4b). Since Pt is still detectable by XPS in the ~10 nm nearest the nanorod surface, we conclude that only a limited amount of Ru is added by UPD (Figure S4). We also note that the EDX signal from Ru, though low in intensity, is constant across the Ru-Pt-BMG(42) nanorod, indicating uniform coverage (Figure 4c).

The methanol oxidation activity of Ru-Pt-BMG(42) was evaluated by cyclic voltammetry in a solution of 0.5 M H_2SO_4 containing 2 M methanol (Figure 4d). A negative shift in onset potentials (by 20 mV) is consistent with the presence of Ru-promoted oxygenate groups discussed in previous reports[42], and suggests good dispersion of Ru and Pt across the BMG surface. We also highlight a ~60% increase in MOR current density after UPD, which confirms the efficacy of Ru addition. The electrochemical stability of Ru-Pt-BMG(42) was evaluated using an accelerated durability test and compared to commercially available PtRu/C (1:1 Pt:Ru ratio) (Figure S5). As with Pt-BMG(42)-catalyzed ORR, we show a higher specific activity for the BMG-based catalyst compared to the supported catalyst (23 vs. 7.9 A mg_{Pt}^{-2})

(Figure S5b). We suggest that additive modification of BMGs with UPD and GD yields better surface dispersion of active elements than traditional bimetallic nanoparticle synthesis methods. Though Ru deposition is used as a model additive process here, a number of elements (i.e. Rh, Ir) could also be combined in this way to enhance catalytic properties.

Additive Modification: Electrodeposition

Among numerous nanostructured pseudo-capacitive electrode architectures, one-dimensional (1D) core-shell designs stand out for their high interfacial area, facilitating electron transport and ion diffusion[43],[44]. Benefitting from the excellent formability of Pt-BMGs, we demonstrate the potential of MnO_x-coated Pt-BMG(57) nanorod arrays for pseudo-capacitive applications. Manganese oxide (MnO_x) is a particularly attractive material for this study due to its high specific capacitance and low cost vs. more common RuO_2 [45].

We show a schematic illustration of the generation of MnO_x-Pt-BMG(57) nanorod arrays (Figure 5a). The core-shell nanostructure is fabricated by electrodepositing MnO_x from dissolved $Mn(CH_3COO)_2$ precursor at 0.4 V (vs. SCE) onto a Pt-BMG(57) array. SEM images show that electrodeposited MnO_x around 20nm conformally covers the BMG nanostructure, resulting in a high surface area electrode (Figure 5b and 5c). XPS spectra of the Pt 4f region were obtained before and after Ar ion milling of the MnO_x to show that the MnO_x coating is defect-free (Figure S6). The presence of Mn 2p peaks (Figure 5d) along with the appearance of multiple features in the O 1s spectrum (Figure 5e) indicate that the MnO_x layer is composed of Mn in several states of oxygen coordination (i.e. Mn-O and Mn-OH), a product of the aqueous-based deposition procedure.

Cyclic voltammograms of the MnO_x-Pt-BMG(57) nanorod array exhibit a rectangular charge/discharge profile, suggesting good charge storage capability (Figure 5f). Due to the

use of a high surface area BMG nanorod scaffold, the coated array exhibits a specific capacitance 2.1 times higher than that of a MnO_x-Pt-BMG(57) flat disc (17.95 vs. 8.54 mF/cm^2 at 5 mV/s) (Figure 5g). A similar trend is found with bare Pt-BMG(57) arrays and Pt-BMG(57) flat discs, although the behavior in this instance involves double-layer capacitance and not pseudo-capacitance (Figure S7).

Though Pt-BMGs are known to exhibit some of the best forming abilities of any metallic glass, they are not an ideal scaffold for pseudo-capacitors in terms of cost. Nevertheless, with the development of new lower-cost BMG compositions, the electrodeposition method shown here could provide a viable route to the high-throughput generation of these and similar devices requiring large surface areas. Furthermore, adding active material onto nanomoulded BMG arrays provides a tunable parameter to control feature sizes and shapes merely by exchanging the BMG template.

Conclusions

In summary we demonstrate and characterize the precise control over catalyst surface composition and structure of free standing platinum based metallic glass nanorods formed using a scalable top-down thermoplastic forming process. Through both subtractive (dealloying) and additive modification techniques (underpotential deposition, galvanic displacement and electrodeposition), we extend the electrochemical applications with elements outside the glass forming ability range. We show that the metallic glass can serve as an ideal platform as a highly active and durable catalyst for hydrogen evolution, oxygen reduction, and methanol oxidation reactions. Furthermore, we suggest that superb formability of metallic glass could open up new application areas as a high surface area support for pseudocapacitor applications. We believe this is just the beginning of numerous possibilities for metallic glass nanostructures and techniques demonstrated here can be further extended

for a wide variety of target reactions ranging from other electrochemical reactions to sensors to surface coatings for enhanced durability or biocompatibility.

Experimental Section

BMG Nanostructure

Bulk metallic glass nanorods were fabricated using a top-down process for all the samples. First, high purity platinum, phosphorous, copper, and nickel were melted in vacuum-sealed silica tubes to form an amorphous disc, as described in our previous work.[16, 17, 18] The fabricated disc was then hot pressed against an anodized aluminum oxide (AAO) template with 200 nm diameter pores. The BMG disc with attached wires/rods was removed from the AAO template using a KOH etch. In order to remove the wires from the disc and make them free-standing, the molded sample was immersed in isopropyl alcohol and water in a 5:1 ratio and placed in a bath sonicator for 4 hours. The free-standing material remained dispersed in the solution and used as an ink. Aliquots of 5, 10 or 20 μL were deposited on top of a glassy carbon electrode and dried at room temperature to form the electrodes for electrochemical characterization.

The ternary (Pt-Cu-Ni) wafer library was made by co-deposition magnetron sputtering onto 100 mm diameter Si(100) wafers using three 50 mm diameter elemental targets, as described in our previous work.[24] Briefly, the base pressure before sputtering is less than 10^{-5} Pa, and the working pressure is kept constant at 0.3 Pa. The compositional gradient was controlled by the target-to-substrate geometry based on the deposition rates measured with a quartz crystal thickness monitor. The thickness of the film library was controlled by the deposition time on the base of deposition rate measurement. Compositions of the library were measured using energy dispersive X-ray spectrum attached to a scanning electron microscope.

Loading measurements were accomplished by analyzing the free-standing material (dissolved in concentrated HNO_3 and HCl) by an inductively coupled plasma mass spectrometer (ICP-MS) (Table S1), as previously calibrated.[37]

Dealloying Procedure

The dealloying procedure was carried out in 0.5 M H_2SO_4 purged with nitrogen using cyclic voltammetry at a sweep rate of 50 mV/s between -0.2 V and 1.2 V vs. Ag/AgCl at room temperature. The scans were recorded every 100 cycles at 50 mV/s and every 200 cycles at 20 mV/s. Since the contribution to the ECSA from the gradually dissolved Cu and Ni is relatively trivial than Pt (Figure 1d-e), the electrochemically active surface area was calculated from the H_2 desorption peak of the CV cycle, from the coulombic charge for hydrogen desorption, assuming a value of 210 $\mu C.cm^{-2}$ Pt for the oxidation of adsorbed atomic H on a smooth Pt surface.[13]

Deposition of Ru

Ruthenium underpotential deposition was conducted using a chronoamperometric technique with dealloyed Pt-BMG(42) after 2000 cycles. The dealloyed nanorods were deposited on a glassy carbon electrode and dipped into a solution of 0.5 M H_2SO_4 and 5 mM of $RuCl_3$. The potential was fixed at 0.58 V vs. Ag/AgCl for 5 minutes. Subsequently the electrode was thoroughly washed with DI water and used for methanol oxidation.

The galvanic displacement reaction with ruthenium followed a similar procedure as UPD, but without the application of voltage. The reaction was monitored by reading the open circuit voltage of Pt-BMG(42) nanorods deposited on a glassy carbon electrode and immersed in a solution of 10 mM $RuCl_3$ in 0.1 M HCl. After displacement the electrode was thoroughly washed with DI water and subsequently cycled in 0.5 M H_2SO_4 to eliminate adsorbed chloride

and to perform the dealloying of the surface until a constant voltammetric profile was reached. The resulting electrode was used for methanol oxidation.

Pseudo-capacitive Electrodes

Pseudo-capacitive electrodes were prepared by applying a positive potential of 0.4 V (vs. SCE) to an array of Pt-BMG(57) nanorods in a solution mixture of 0.1 M manganese acetate and 0.1 M sodium sulfate at room temperature. The residual solution in nanorod arrays was removed by rinsing with DI water. Cyclic voltammetry curves were measured in a three-electrode cell at different scan rates with a Ag/AgCl reference electrode and a platinum counter-electrode in a potential range between 0 and 0.8 V in a 1 M Na_2SO_4 electrolyte.

Electrochemical Characterization

Electrochemical investigations were carried out in 0.5 M H_2SO_4 solution purged with nitrogen using cyclic voltammetry with a sweep rate of 50 mV/s between -0.2 V and 1.2 V vs. Ag/AgCl at room temperature. All the experiments were made in a three-electrode configuration using a pure platinum mesh as a counter electrode, an Ag/AgCl reference electrode from Pine Instruments and a glassy carbon working electrode. The oxygen reduction reaction (ORR) was performed in an O_2 saturated 0.5 M H_2SO_4 solution. The curves were recorded on a rotating disc electrode from 400 to 2500 rpm by sweep voltammetry with a rate of 5 mV/s from 1.2 V to -0.1 V vs. Ag/AgCl. For the methanol oxidation reaction a solution of 0.5 M H_2SO_4 containing 2 M methanol, purged with nitrogen, was used. The reaction was investigated by recording the voltammetry profile at 50 mV/s between -0.2 V and 1.2 V vs. Ag/AgCl.

The accelerated durability test also employed a cyclic voltammetry technique, cycling between 0.4 V and 0.9 V vs. Ag/AgCl at 50 mV/s for a total of 2000 cycles at room

temperature and a more severe experiment at 80°C for a total of 3000 cycles. Voltammograms were recorded at every 50 cycles, between -0.2 V and 1.2 V vs. Ag/AgCl in both experiments, to account for the electrochemically active surface area derived from the hydrogen desorption peaks.

Physical Characterization

Physical characterization of pristine and cycled electrodes was conducted using an FEI Tecnai Osiris 200 kV transmission electron microscope (TEM) and a Hitachi SU-70 scanning electron microscope (SEM) with energy dispersive X-ray spectroscopy (EDX) functions. X-ray photoelectron spectroscopy (XPS) measurements were performed at Brookhaven National Laboratory on a SPECS GmbH instrument under ultrahigh vacuum (UHV) conditions. The X-ray source was Al Kα at a power of 300 W. Data were collected for C 1s, O 1s, Pt 4f, and Ru 3d with a pass energy of 25 eV. Binding energies were calibrated to the C 1s photoemission peak of adventitious hydrocarbons at 285.0 eV. Peak locations and peak widths were obtained using a Shirley background subtraction and by fitting the data to mixed Gaussian−Lorentzian line shapes (CasaXPS).

Supporting Information

Supporting Information is available from the Wiley Online Library

Acknowledgements

Gustavo Doubek, Ryan C. Sekol and Jinyang Li contributed equally to this work. The authors are grateful for support from NSF under Grant No. MRSEC DMR 1119826 (CRISP). A.D.T. also thanks the AFOSR (FA9550-11-1-0219) and NSF-CAREER award (CBET-0954985). W.-H. R. thanks The NatureNet Program of The Nature Conervancy. Facilities use was supported by YINQE, NSF MRSEC DMR 1119826 (CRISP). Research was carried out in part at the Center for Functional Nanomaterials, Brookhaven National Laboratory, which is

supported by the U.S. Department of Energy, Office of Basic Energy Sciences, under Contract DE-AC02-98CH10886.

Received: ((will be filled in by the editorial staff))
Revised: ((will be filled in by the editorial staff))
Published online: ((will be filled in by the editorial staff))

[1] S. Wasmus, A. Kuver, J Electroanal Chem 1999, 461, 14; A. S. Aricò, P. Bruce, B. Scrosati, J.-M. Tarascon, W. van Schalkwijk, Nature Materials 2005, 4, 366.

[2] M. Carmo, D. L. Fritz, J. Merge, D. Stolten, Int J Hydrogen Energ 2013, 38, 4901.

[3] J. Suntivich, H. A. Gasteiger, N. Yabuuchi, H. Nakanishi, J. B. Goodenough, Y. Shao-Horn, Nat Chem 2011, 3, 647; F. S. Gittleson, W.-H. Ryu, A. D. Taylor, ACS Applied Materials & Interfaces 2014, 6, 19017; W.-H. Ryu, F. S. Gittleson, M. Schwab, T. Goh, A. D. Taylor, Nano Lett 2015, 15, 434; F. S. Gittleson, R. C. Sekol, G. Doubek, M. Linardi, A. D. Taylor, Physical Chemistry Chemical Physics 2014, 16, 3230; Y.-C. Lu, H. A. Gasteiger, Y. Shao-Horn, Journal of the American Chemical Society 2011, 133, 19048.

[4] T. Palaniselvam, M. O. Valappil, R. Illathvalappil, S. Kurungot, Energy & Environmental Science 2014, 7, 1059; V. R. Stamenkovic, B. S. Mun, M. Arenz, K. J. J. Mayrhofer, C. A. Lucas, G. Wang, P. N. Ross, N. M. Markovic, Nature Materials 2007, 6, 241.

[5] M. K. Debe, Nature 2012, 486, 43.

[6] J. Greeley, I. E. L. Stephens, A. S. Bondarenko, T. P. Johansson, H. A. Hansen, T. F. Jaramillo, J. Rossmeisl, I. Chorkendorff, J. K. Nørskov, Nat Chem 2009, 1, 552.

[7] D. Wang, H. L. Xin, R. Hovden, H. Wang, Y. Yu, D. A. Muller, F. J. DiSalvo, H. D. Abruña, Nature Materials 2012, 12, 81; X. Wang, S.-I. Choi, L. T. Roling, M. Luo, C. Ma, L. Zhang, M. Chi, J. Liu, Z. Xie, J. A. Herron, M. Mavrikakis, Y. L. Zhang, L. T. Roling, X. Wang, M. Vara, M. Chi, J. Liu, S. I. Choi, J. Park, J. A. Herron, Z. Xie, M. Mavrikakis, Y. Xia, Science 2015, 349, 412; Xia, Nature Communications 2015, 6, 7594;

[8] D. F. van der Vliet, C. Wang, D. Tripkovic, D. Strmcnik, X. F. Zhang, M. K. Debe, R. T. Atanasoski, N. M. Markovic, V. R. Stamenkovic, Nature Materials 2012.

[9] Y.-X. Chen, S.-P. Chen, Z.-Y. Zhou, N. Tian, Y.-X. Jiang, S.-G. Sun, Y. Ding, Z. L. Wang, Journal of the American Chemical Society 2009, 131, 10860.

[10] Z. Chen, Y. Yang, S. Kumar, G. Lu, The Journal of Physical Chemistry C 2014, 118, 28609.

[11] Y. Feng, H. Liu, P. Wang, F. Ye, Q. Tan, J. Yang, Scientific Reports 2014, 4, 6204.

[12] Z. Peng, J. Wu, H. Yang, Chemistry of Materials 2010, 22, 1098.

[13] G. Kumar, H. X. Tang, J. Schroers, Nature 2009, 457, 868 ; A. D. Taylor, B. D. Lucas, L. J. Guo, L. T. Thompson, Journal of Power Sources 2007, 171, 218.

[14] D. C. Hofmann, Journal of Materials 2013, 2013, 1.

[15] P. Hojati-Talemi, M. A. Gibson, D. East, G. P. Simon, Applied Physics Letters 2011, 99, 194104.

[16] M. Carmo, R. C. Sekol, S. Ding, G. Kumar, J. Schroers, A. D. Taylor, ACS Nano 2011, 5, 2979.

[17] S. Mukherjee, M. Carmo, G. Kumar, R. C. Sekol, **A. D. Taylor**, J. Schroers, Electrochimica Acta 2012, 74, 145.

[18] S. Mukherjee, R. C. Sekol, M. Carmo, E. I. Altman, **A. D. Taylor**, J. Schroers, Advanced Functional Materials 2013, 74, 145; R. C. Sekol, M. Carmo, G. Kumar, F. Gittleson, G. Doubek, K. Sun, J. Schroers, **A. D. Taylor**, Int J Hydrogen Energ 2013, 38, 11248.

[19] R. C. Sekol, G. Kumar, M. Carmo, F. Gittleson, N. Hardesty-Dyck, S. Mukherjee, J. Schroers, **A. D. Taylor**, Small 2012, n/a.

[20] M. Zhao, K. Abe, S.-i. Yamaura, Y. Yamamoto, N. Asao, Chemistry of Materials 2014, 26, 1056.

[21] Y. Yang, T. Adit Maark, A. Peterson, S. Kumar, Phys. Chem. Chem. Phys. 2015, 17, 1746.

[22] J. Lee, A. Urban, X. Li, D. Su, G. Hautier, G. Ceder, Science 2014, 343, 519; B. Zberg, P. J. Uggowitzer, J. F. Loffler, Nature Materials 2009, 8, 887.

[23] W. E. Brower, M. S. Matyjaszczyk, T. L. Pettit, G. V. Smith, Nature 1983, 301, 497; J.-W. Jung, W.-H. Ryu, J. Shin, K. Park, I.-D. Kim, ACS Nano 2015, 9, 6717.

[24] S. Y. Ding, Y. H. Liu, Y. L. Li, Z. Liu, S. Sohn, F. J. Walker, J. Schroers, Nature Materials 2014, 13, 494.

[25] P. Strasser, S. Koh, T. Anniyev, J. Greeley, K. More, C. Yu, Z. Liu, S. Kaya, D. Nordlund, H. Ogasawara, M. F. Toney, A. Nilsson, Nat Chem 2010, 2, 454.

[26] P. Strasser, Rev Chem Eng 2009, 25, 255.

[27] B. Han, C. E. Carlton, A. Kongkanand, R. S. Kukreja, B. R. Theobald, L. Gan, R. O'Malley, P. Strasser, F. T. Wagner, Y. Shao-Horn, Energy Environ. Sci. 2015, 8, 258.

[28] Q. Chen, K. Sieradzki, Nature Materials 2013, 12, 1102.

[29] H. W. Pickering, Corrosion Science 1983, 23, 1107.

[30] J. Erlebacher, M. J. Aziz, A. Karma, N. Dimitrov, K. Sieradzki, Nature 2001, 410, 450.

[31] J. Schroers, Advanced Materials 2010, 22, 1566.

[32] A. J. Bard, L. R. Faulkner, *Electrochemical Methods Fundamentals and Applications*, Jonh Wiley & Sons, Inc., 2001.

[33] T. Aburada, J. M. Fitz-Gerald, J. R. Scully, Corrosion Science 2011, 53, 1627.

[34] C. Cui, L. Gan, M. Heggen, S. Rudi, P. Strasser, Nature Materials 2013, 12, 765.

[35] A. D. Taylor, M. Michel, R. C. Sekol, J. M. Kizuka, N. A. Kotov, L. T. Thompson, Advanced Functional Materials 2008, 18, 3354.

[36] C. A. Reiser, L. Bregoli, T. W. Patterson, J. S. Yi, J. D. L. Yang, M. L. Perry, T. D. Jarvi, Electrochem Solid St 2005, 8, A273.

[37] R. C. Sekol, X. Li, P. Cohen, G. Doubek, M. Carmo, A. D. Taylor, Applied Catalysis B: Environmental 2013, 138–139, 285.

[38] C. Xu, L. Wang, X. Mu, Y. Ding, Langmuir 2010, 26, 7437; X. Wang, J. Liao, C. Liu, W. Xing, T. Lu, Electrochemistry Communications 2009, 11, 198; K.-W. Park, Y.-E. Sung, The Journal of Physical Chemistry B 2005, 109, 13585; M. Watanabe, S. Motoo, Journal of Electroanalytical Chemistry and Interfacial Electrochemistry 1975, 60, 267.

[39] C. H. Cui, S. H. Yu, Accounts Chem Res 2013, 46, 1427.

[40] H. Yang, Y. Yang, S. Zou, The Journal of Physical Chemistry C 2007, 111, 19058.

[41] J. Y. Shen, A. Adnot, S. Kaliaguine, Applied Surface Science 1991, 51, 47.

[42] L. Li, Y. Xing, Energies 2009, 2, 789; L. Gancs, B. N. Hult, N. Hakim, S. Mukerjee, Electrochemical and Solid-State Letters 2007, 10, B150; T. Huang, S. Mao, G. Zhou, Z. Zhang, Z. Wen, X. Huang, S. Ci, J. Chen, Nanoscale 2015, 7, 1301.

[43] J. R. McDonough, J. W. Choi, Y. Yang, F. La Mantia, Y. G. Zhang, Y. Cui, Applied Physics Letters 2009, 95.

[44] C. C. Hu, K. H. Chang, M. C. Lin, Y. T. Wu, Nano Lett 2006, 6, 2690.

[45] J. P. Liu, J. Jiang, C. W. Cheng, H. X. Li, J. X. Zhang, H. Gong, H. J. Fan, Advanced Materials 2011, 23, 2076; X. H. Xia, J. P. Tu, Y. Q. Zhang, X. L. Wang, C. D. Gu, X. B. Zhao, H. J. Fan, Acs Nano 2012, 6, 5531; M. K. Song, S. Cheng, H. Y. Chen, W. T. Qin, K. W. Nam, S. C. Xu, X. Q. Yang, A. Bongiorno, J. Lee, J. M. Bai, T. A. Tyson, J. Cho, M. L. Liu, Nano Lett 2012, 12, 4416.

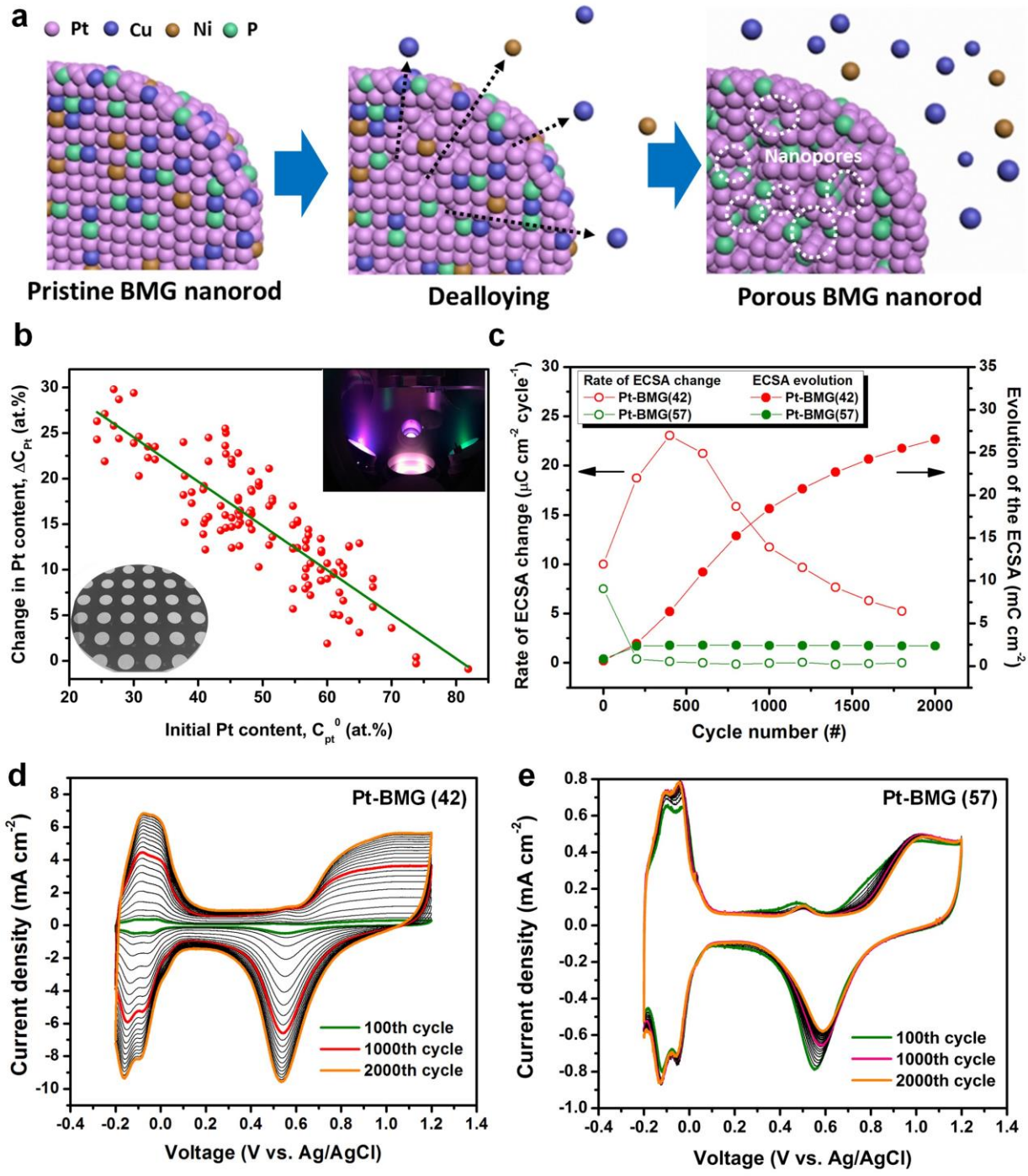

Figure 1 Evolution of the Pt-BMG surface as a result of dealloying: (a) Schematic drawing showing nanopore formation upon dealloying. (b) The change in Pt content due to dealloying (ΔC_{Pt}) as a function of initial Pt content (C_{Pt}^0), characterized in a high-throughput manner by EDX. Insets (left) Pt-Ni-Cu alloy compositional spread on Si wafer, (right) co-sputtering

system. (c) Evolution of the electrochemical surface area (ECSA) of Pt-BMGs during cycling in 0.5 M H_2SO_4. (d-e) Cyclic voltammograms of Pt-BMGs over 2000 cycles.

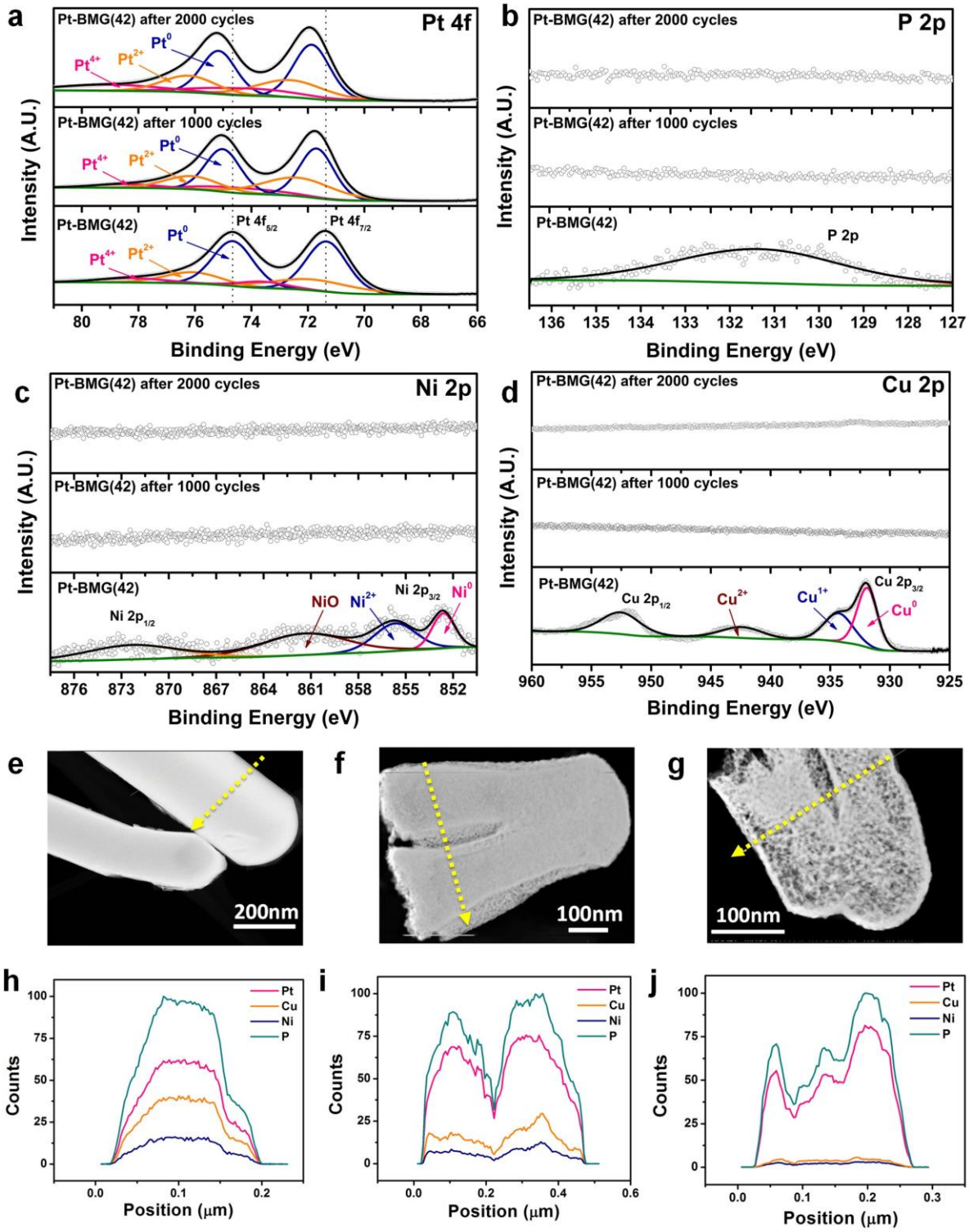

Figure 2 Surface characterization of dealloyed Pt-BMGs: X-ray photoelectron spectra (XPS) for (a) Pt 4f, (b) P 2p, (c) Ni 2p and (d) Cu 2p of Pt-BMG(42), Pt-BMG(42) after 1000 cycles and Pt-BMG(42) after 2000 cycles. (e-g) HAADF images taken at 0^{th}, 1000^{th} and 2000^{th} cycles, (h-j) EDX line scans of free-standing nanorods corresponding to the HAADF images above.

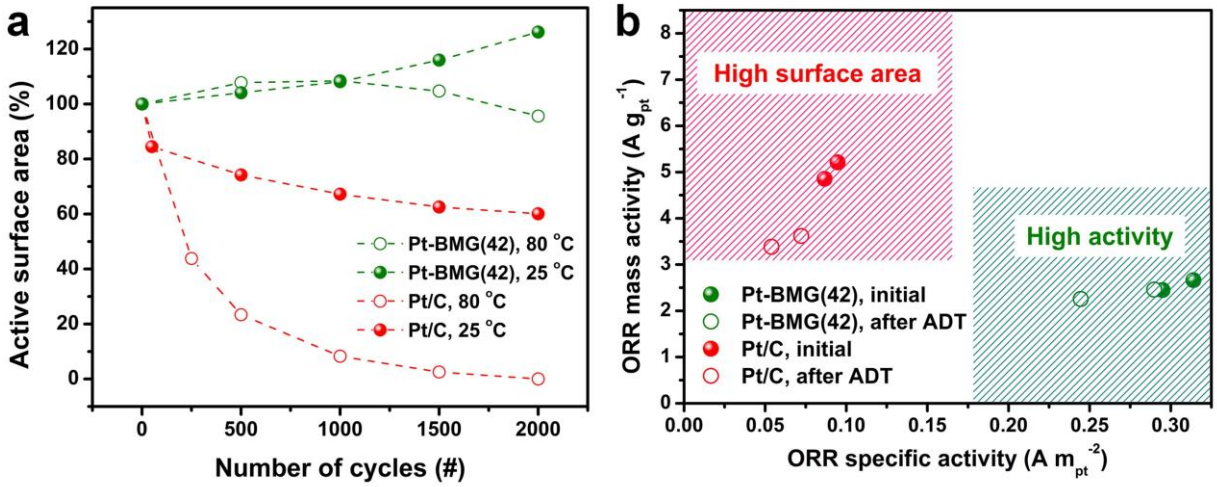

Figure 3 (a) Hydrogen desorption ECSA change at 25°C and 80°C, cycling performed in 0.5 M H2SO4. (b) Mass and specific activities of Pt-BMG(42) and Pt/C, measured with a rotating disc electrode at 0.8 V vs. RHE before and after accelerated durability testing (ADT).

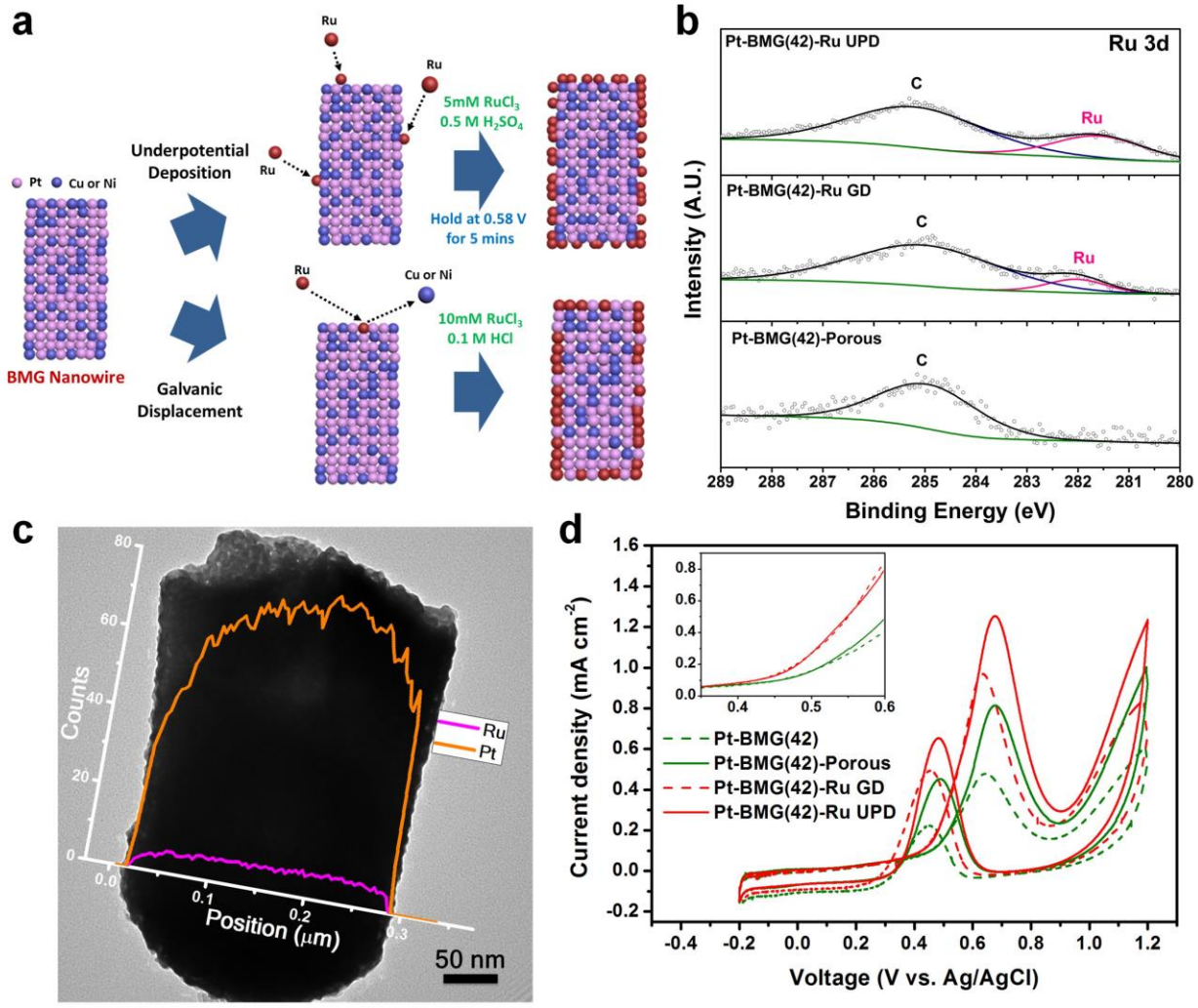

Figure 4 (a) Schematic drawing showing the two methods for surface modification over the original Pt-BMG(42) leading to the Ru incorporation. (b) Ru 3d XPS spectra of dealloyed Pt-BMG(42), after UPD and GD. (c) TEM picture coupled with an EDX-line scan of dealloyed Pt-BMG(42) after UPD indicating Pt and Ru signals. (d) Cyclic voltammograms for methanol oxidation on the Pt-BMG(42) nanorods after Ru deposition by UPD and GD.

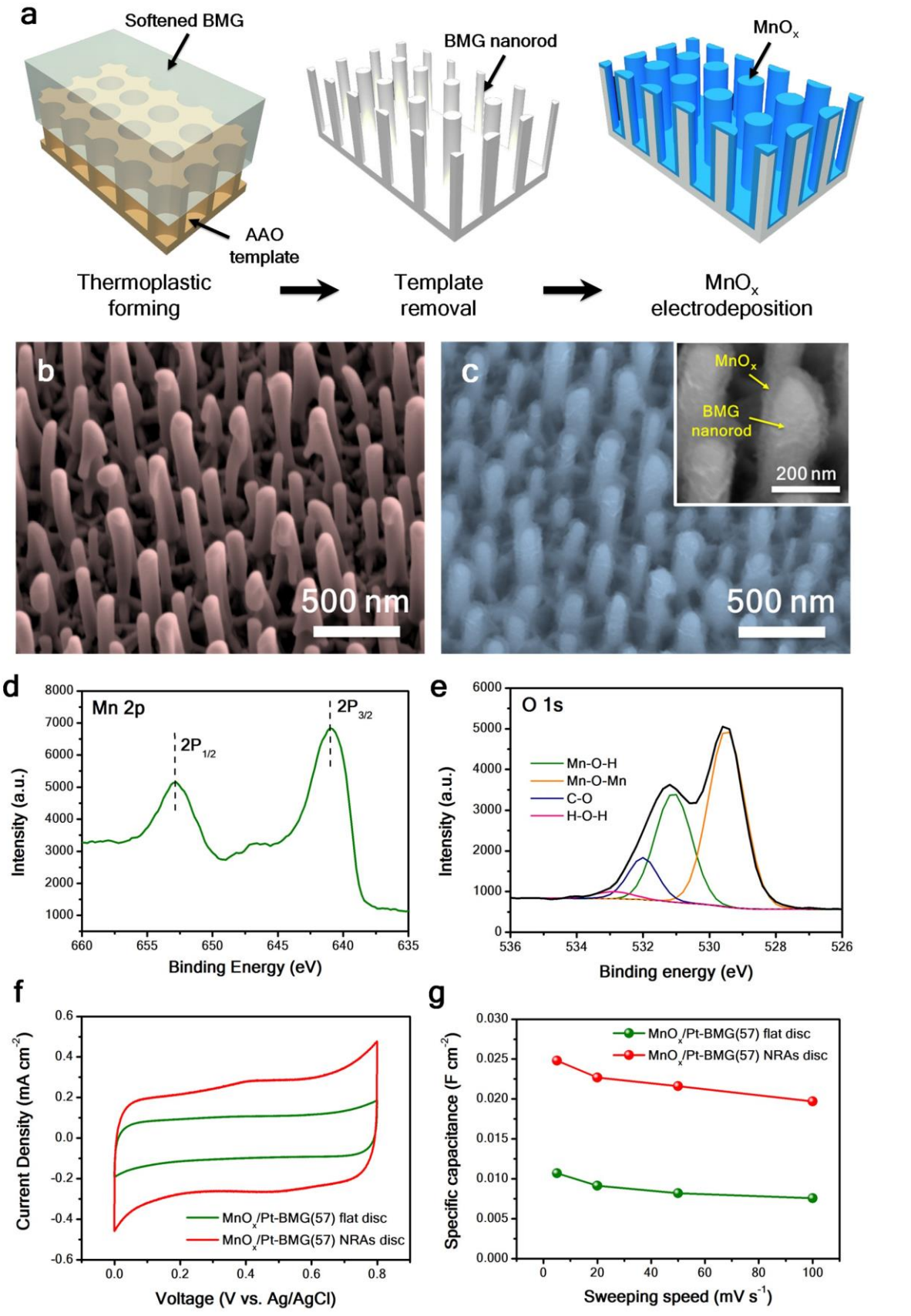

Figure 5 (a) Schematic illustration for the fabrication processes of MnO_x-Pt-BMG(57) nanorod arrays. (b) SEM image of Pt-BMG(57) array. (c) SEM image of MnO_x-Pt-BMG(57)

array. (d) XPS Mn 2p spectrum of MnO_x-Pt-BMG(57) array. (e) XPS O 1s spectrum of MnO_x-Pt-BMG(57) array with deconvoluted peaks. (f) Cyclic voltammograms in 1M Na_2SO_4 at a scan rate of 50 mV/s. (h) Specific capacitance vs. scan rate for MnO_x-coated BMG array and flat discs.

Electrochemical devices such as fuel cells, electrolyzers, lithium-air batteries, and pseudo-capacitors are expected to play a major role in energy conversion/storage in the near future. We demonstrate how desirable BMG compositions can be obtained using a combinatorial approach and show that these alloys can serve as a platform technology for a wide variety of electrochemical applications through several surface modification techniques.

Bulk metallic glass, nanomaterial, electrocatalyst, surface modification, pesudocapacitor Keyword

Gustavo Doubek†, Ryan C. Sekol†, Jinyang Li†, Won-Hee Ryu, Forrest S. Gittleson, Siamak Nejati, Eric Moy, Candy Reid, Marcelo Carmo, Marcelo Linardi, Punnathat Bordeenithikasem, Emily Kinser, Yanhui Liu, Xiao Tong, Chinedum Osuji, Jan Schroers, Sundeep Mukherjee, and André D. Taylor*

† These authors contributed equally to this work.

Guided Evolution of Bulk Metallic Glass Nanostructures: A Platform for Designing Three-Dimensional Electrocatalytic Surfaces